VISCOACOUSTIC FULL WAVEFORM INVERSION FOR SPATIALLY CORRELATED AND UNCORRELATED PROBLEMS IN REFLECTION SEISMICS

R. Shigapov, A. Kurzmann, and T. Bohlen

email: *r.shigapov@spbu.ru, kurzmann@kit.edu*

keywords: *viscoacoustic full waveform inversion, time-domain, attenuation*

ABSTRACT

Attenuation and dispersion of elastic waves play important role in real Earth and contain valuable information about the subsurface. To recover spatial distributions of both velocity and attenuation, in this work we develop viscoacoustic full waveform inversion (FWI) and investigate its applicability on synthetic marine reflection data. We use finite-difference solution of 2D time-domain viscoacoustic equations using relaxation mechanisms of the generalized standard linear solid (GSLS). Viscoacoustic FWI is a multiparameter inverse problem, and suffers from the cross-talk between different parameter classes. To investigate the cross-talk, we compared both sequential and parallel inversion strategies using spatially correlated and uncorrelated models of velocity and attenuation. Our numerical results based on the 1D layered and 2D Marmousi models show good reconstruction of velocity at whole grid and satisfactory reconstruction of attenuation only in the upper part of model. Although in all cases the inverted Q values in the lowest part of model are far away from the true ones, we observe improvements in the velocity reconstruction and an excellent fit of synthetic and recorded seismograms. This can be interpreted either as low sensitivity of the synthetic reflection marine data to attenuation properties of the lowest part of model or as cross-talk where attenuation-related data misfit is explained by the velocity model.

INTRODUCTION

A lot of of experimental data confirm that real media are far from to be pure elastic. In fact, attenuation and dispersion of elastic waves play important role and need to be taken into account. However, a half a century after publishing the paper "Q" by Knopoff (1964) our understanding of attenuation mechanisms (Müller et al., 2010) and ability to get reliable Q estimates (Kamei and Pratt, 2013) are still limited. The problem is compounded by the fact that scattering effects mimic intrinsic attenuation (Shapiro and Hubral, 1999). This opens the main research question of our study: can spatial distributions of velocity and intrinsic attenuation be accurately inverted by applying full waveform inversion (FWI) to reflection data?

Full waveform inversion is the state-of-the-art technology for retrieving elastic parameters of a subsurface via iterative minimization of the difference between the modelled and recorded wavefields (Virieux and Operto, 2009). Based on local gradient optimization, FWI becomes highly efficient due to the adjoint-state calculation of a gradient (Plessix, 2006) introduced in geophysics by Lailly (1983) and Tarantola (1984). At the moment there are already several applications of viscoacoustic FWI to field data (Malinowski et al., 2011; Prieux et al., 2013) and laboratory (Watanabe et al., 2004). Theoretical basis of FWI in a general anisotropic viscoelastic medium was first formulated by Tarantola (1988) in time domain. However, since the first numerical implementations of viscoacoustic FWI (Song et al., 1995; Liao and McMechan, 1996; Hicks and Pratt, 2001) until the most recent ones (Long et al., 2009; Malinowski et al., 2011; Hak and Mulder, 2011; Brossier, 2011; Kamei and Pratt, 2013; Prieux et al., 2013; Liu et al., 2013; Takougang

and Calvert, 2013) both the modeling and inversion parts were mostly developed in the frequency domain. Among the benefits of frequency-domain modeling and inversion are easy implementation of attenuation using complex-valued frequency-dependent velocities, computation of gradients for velocity and Q without extra-cost, and natural use of a multiscale strategy meaning sequential inversion from low to high frequencies. Time-domain FWI in attenuative media is less popular (Charara et al., 2000; Askan et al., 2007; Askan and Bielak, 2008; Askan et al., 2010; Assimaki et al., 2012; Bai et al., 2014; Ren et al., 2014). First, implementation of strictly constant Q within a wide frequency band is not so easy in time domain as in the frequency domain. Indeed, the simplest viscoacoustic formulations (Liu et al., 2013) are based on the frequency-dependent attenuation mechanisms. To get approximately constant Q for a given frequency band, we have to consider a sum of relaxation mechanisms (Liu et al., 1976). From other side, an advantage of time-domain implementations is effective parallelization of computations. An alternative strategy can be a combination of time-domain modeling and frequency-domain inversion (Causse et al., 1999). Summarizing a brief review of viscoacoustic inversion, we point out that the mentioned papers deal mainly with inversion of spatially correlated velocity and attenuation structures which means the shapes of models of different parameters are the same. The most important exception is the paper by Kamei and Pratt (2013), however, it was done for a cross-hole geometry with a relatively good illumination.

In this paper we implement time-domain viscoacoustic FWI and investigate its applicability on synthetic marine reflection data. First, we explain theory of viscoacoustic modeling and inversion, and describe briefly implementation of the code. Then, we show a few numerical results using different spatially correlated and uncorrelated models of velocity and attenuation.

THEORY AND IMPLEMENTATION

Forward viscoacoustic modeling

In time domain a general linear viscoacoustic equation of motion consists of a convolutional kernel representing Bolzmann's superposition principle (Carcione, 2007). This integro-differential equation with a kernel of a general kind is not convenient for numerical calculation. With the exponentional kernel corresponding to the relaxation mechanism called standard linear solid (SLS) the integro-differential equation can be reformulated as a system of differential equations with a new "memory variable" (Carcione et al., 1988; Robertsson et al., 1994). Then, the conventional constant Q model, i.e., $Q_{\mathrm{P}}(\omega) = const. = Q_{\mathrm{P},0}$ with frequency ω, can be approximated by a set of SLSs – generalized SLS (GSLS) – within the given frequency band (Liu et al., 1976). GSLS is defined using L relaxation times $\tau_{\sigma,l}$ and L retardation times $\tau_{\epsilon,l}$. While an acoustic model is characterized by the parameters density ρ and bulk modulus κ, the viscoacoustic medium is defined by ρ, the relaxed bulk modulus κ_r and additional $2L$ relaxation parameters $\tau_{\sigma,l}$ and $\tau_{\epsilon,l}$ ($l = \{1, \ldots, L\}$). We follow Blanch et al. (1995) to reduce a number of parameters in GSLS from $2L$ to $L+1$. Finally, we solve a system of $3+L$ differential equations for a two-dimensional viscoacoustic medium:

$$\begin{aligned}
&\dot{p}\left(\mathbf{x},t\right) - K_r\left(\mathbf{x}\right)\nabla\cdot\mathbf{w}\left(\mathbf{x},t\right) - \sum_{l=1}^{L} r_l\left(\mathbf{x},t\right) = \delta\left(\mathbf{x}-\mathbf{x}_s\right)s\left(t\right),\\
&\dot{\mathbf{w}}\left(\mathbf{x},t\right) = -\frac{1}{\rho\left(\mathbf{x}\right)}\nabla p\left(\mathbf{x},t\right),\\
&\dot{r_l}\left(\mathbf{x},t\right) = -\frac{1}{\tau_{\sigma,l}}\left(\kappa_r\tau_{\mathrm{P}}\left(\mathbf{x}\right)\nabla\cdot\mathbf{w}\left(\mathbf{x},t\right) + r_l\left(\mathbf{x},t\right)\right), \qquad l = 1, ..., L.
\end{aligned} \tag{1}$$

where $K_r\left(\mathbf{x}\right) = \kappa_r\left(\mathbf{x}\right)\left(1 + L\tau_{\mathrm{P}}\left(\mathbf{x}\right)\right)$, p denotes a scalar field of pressure, $\mathbf{w}$ is a vector field of particle velocities, r_l stands for l-th scalar memory variable, L is the number of relaxation mechanisms, τ_{P} is a relaxation parameter introduced by Blanch et al. (1995), $\delta\left(\mathbf{x}-\mathbf{x}_s\right)$ is a delta function with the non-zero value at the source position $\mathbf{x}_s$, $s\left(t\right)$ denotes source time function, ρ means density, and the upper dot denotes time derivative. The relation (Emmerich and Korn, 1987; Blanch et al., 1995) between τ_{P} and Q_{P} can be approximated by:

$$\frac{1}{\tau_{\mathrm{P}}} = \sum_{l=1}^{L}\frac{\omega_0/\omega_{\mathrm{r},l}}{1+\omega_0^2/\omega_{\mathrm{r},l}^2}\,Q_{\mathrm{P},0} \quad \text{for} \quad Q_{\mathrm{P},0} \gg 1, \tag{2}$$

where $\omega_{\mathrm{r},l}$ denote relaxation frequencies $\omega_{\mathrm{r},l} = 2\pi f_{\mathrm{r},l} = \frac{1}{\tau_{\sigma,l}}$ and $\omega_0 = 2\pi f_0$ denotes the reference frequency, at which no attenuation-related dispersion occurs. The system (1) is solved by a time-domain finite-difference time-stepping method (Alford et al., 1974) with perfectly matched layer boundary condition (cp. Berenger, 1994; Chew and Weedon, 1994) and heavy parallelization (Bohlen, 2002; Kurzmann et al., 2009) as implemented by Kurzmann et al. (2013).

Inversion via local optimization

The inverse problem of finding the vector $\mathbf{m}(\mathbf{x}) = [\mathbf{v}_{\mathrm{p}}(\mathbf{x}), \mathbf{Q}_{\mathrm{p}}(\mathbf{x})]$ of model parameters is formulated as a minimization problem using the conventional L_2-norm of a misfit between the modelled p and observed p_{obs} pressure fields:

$$E(\mathbf{m}) = \sum_{s=1}^{N_s} \sum_{r=1}^{N_r} \sum_{j=1}^{N_t} ||p^{s,r}(t_j;\mathbf{m}) - p_{\mathrm{obs}}^{s,r}(t_j)||_2^2 , \tag{3}$$

where N_s, N_r, and N_t denote number sources, receivers, and time steps correspondingly. Although the parameters of interest are velocity v_{P} and quality factor Q_{P}, our implementation of viscoacoustic equations requires parameter τ_{P} rather Q_{P}. However, since Q_{P} ranges over few orders of magnitude, we prefer to invert $\log(\tau_{\mathrm{P}})$ rather Q_{P}. We derived gradients of the misfit function with respect to v_{P} and $\log(\tau_{\mathrm{P}})$ using the adjoint-state method (Plessix, 2006):

$$g_{[v_{\mathrm{P}}]} = \int \left(v_{\mathrm{P}} \rho \left(1 + L\ \tau_{\mathrm{P}}\right) \nabla \cdot \mathbf{w} + \frac{r}{v_{\mathrm{P}}} \right) \hat{p}\ \mathrm{d}t, \tag{4}$$

$$g_{[\log(\tau_{\mathrm{P}})]} = \int \left(v_{\mathrm{P}}^2\ \rho\ L\ \tau_{\mathrm{P}}\ \nabla \cdot \mathbf{w} + r \right) \hat{p}\ \mathrm{d}t, \tag{5}$$

where $\hat{p} = \hat{p}\,(\mathbf{x}, t)$ denotes adjoint pressure field (due to clarity, spatial and temporal dependences are omitted).

We minimize the misfit function using the preconditioned conjugate gradient method applying a wavefield-based preconditioning of both the gradients (Fichtner et al., 2009; Kurzmann et al., 2013). The general model update is given at iteration $n+1$ by

$$[v_{\mathrm{P}}]^{n+1} = [v_{\mathrm{P}}]^n - \mu_{[v_{\mathrm{P}}]}^{n+1}\ g_{[v_{\mathrm{P}}]}^{n+1}, \tag{6}$$

$$[\log(\tau_{\mathrm{P}})]^{n+1} = [\log(\tau_{\mathrm{P}})]^n - \mu_{[\log(\tau_{\mathrm{P}})]}^{n+1}\ g_{[\log(\tau_{\mathrm{P}})]}^{n+1}. \tag{7}$$

The adaptive step lengths $\mu_{[v_{\mathrm{P}}]}$ and $\mu_{[\log(\tau_{\mathrm{P}})]}$ are computed using a parabolic line search algorithm (e.g., Kurzmann et al., 2009). However, the simultaneous inversion for both v_{P} and Q_{P} requires independent step length estimations. On the one hand, this significantly increases computational efforts due to a lot of additional forward modelings, but, on the other hand, it allows the computation of reasonable step lengths. In detail, $\mu_{[v_{\mathrm{P}}]}$ and $\mu_{[\log(\tau_{\mathrm{P}})]}$ may differ by some orders of magnitude which cannot be represented by one single step length.

SYNTHETIC FWI EXPERIMENTS

In this work we apply viscoacoustic inversion to a 1D structured and the 2D Marmousi model. In both cases we investigate its impact on spatially correlated and spatially uncorrelated models of velocity and attenuation. In order to compare and to evaluate results of the Marmousi experiment, we performed an additional quasi-acoustic reference inversion using the Q_{P} model as passive modeling parameter (cp. Kurzmann, A., 2012).

General inversion setup

In the following time-domain viscoacoustic approach the attenuation of a medium is approximated by $L = 3$ relaxation mechanisms within the desired frequency ranges of both experiments – following the rule of one relaxation mechanism per octave (Blanch et al., 1995). L relaxation frequencies

$f_{r,l}$ ($l = \{1, \ldots, L\}$) are estimated from $Q_{P,0}$ and the reference frequency $f_0 = f_s$ using the Q_P-approximation method mentioned above. Depending on the aim of this work, some restrictions are applied:

- We invert only velocity v_P and attenuation Q_P models.
- The density model is assumed to be correct.
- The source signal is assumed to be correct.
- In the following 1D and 2D examples FWT is not allowed to apply model updates within the water layer due to the assumption of known parameters, i.e., $v_\mathrm{P} = 1500\ \frac{\mathrm{m}}{\mathrm{s}}$ and $Q_\mathrm{P} = 200$ in case of 1D experiment (assuming that wavefields are almost insensitive to Q_P values higher than a few hundreds) as well as $Q_\mathrm{P} = 60000$ in case of the Marmousi experiment.
- The algorithm comprises gradient computation based on the L_2 misfit function and the conjugate gradient method (Mora, 1987).
- To avoid unwanted side effects, only a minimum repertoire of preconditioning features is applied: time-wondowing of the data is omitted, low-pass filtering of observed data over multiple stages [Bunks et al. (1995) and analogous to frequency selection in frequency-domain FWT (Sirgue and Pratt, 2004)] is applied in case of Marmousi model, wavefield-based preconditioning (Fichtner et al., 2009; Igel et al., 1996) of the gradient is performed for both 1D and 2D model.

Synthetic 1D experiment

The first example consists of a layered 1D model with a water layer on top, followed by sedimentary rocks with low and high attenuation (Figure 1). It represents an usual case of subsurface properties within a marine environment, i.e., the placement of a highly attenuative layer at top of sedimentary rocks. The acquisition geometry is located at the free surface and consists of 24 explosive sources as well as 278 hydrophones (for each source all receivers are used). The source signal consists of a Ricker wavelet with a peak frequency $f_s = 80$ Hz. The model size is 130×308 m which results – using a grid spacing $DH = 0.5$ m – in a grid size of 260×616 grid points. Due to the application of a perfectly matched layer (width = 15 m) for avoiding artificial boundary reflections in finite-difference modeling, all model related figures are limited to the illustration of the relevant area. Furthermore, the synthetic seismic data is obtained by application of a recording time of 0.21 s with a time discretization of $DT = 8 \cdot 10^{-5}$ s.

The approximation of relaxation parameters are based on reference frequency $f_0 = f_s$. In order to consider the relevant frequency content $f = [0,\ 200]$ Hz of the data we use three relaxation mechanisms with corresponding relaxation frequencies $f_{r,l} = (1.20, 17.6, 179)$ Hz. As discussed by Kurzmann, A. (2012), the missing attenuation in water causes a good match of direct wave and even the seafloor reflection. However, all later reflections are significantly characterized by amplitude decay and dispersion effects.

Regarding the 1D model, several inversion tests have been employed to investigate the sensitivity of viscoacoustic FWI to inversion strategy (sequential or parallel) and spatial correlation of velocity and attenuation (cp. Table 1). For both correlated and uncorrelated problems we perform a joint v_P-Q_P inversion ("parallel") and a sequential inversion (starting with reconstruction of v_P, then continuation with joint inversion). For these inversion tests a set of input models is required:

- True (Figure 1a) and initial (Figure 1b) velocity models are used in all tests.
- Test 1 and Test 2 with spatial correlation of v_P and Q_P are based on true (Figure 2a) and initial (Figure 2b) Q_P models. The corresponding inversion result can be found in Figures 2c,d (Test 1) and 2e,f (Test 2).
- Tests 3 and Test 4 with spatially uncorrelated v_P and Q_P models are based on true (Figure 3a) and initial (Figure 3b) Q_P models. The corresponding inversion result can be found in Figures 3c,d (Test 3) and 3e,f (Test 4).

Table 1: 1D experiment: Compilation of all FWI tests.

	spatial correlation of v_P and Q_P	inversion strategy	initial models
Test 1	correlated	parallel	gradient v_P and gradient Q_P
Test 2	correlated	sequential	gradient v_P and gradient Q_P
Test 3	uncorrelated	parallel	gradient v_P and gradient Q_P
Test 4	uncorrelated	sequential	gradient v_P and gradient Q_P

Test 1 deals with simultaneous inversion of spatially correlated v_P and Q_P. The recovered v_P model (Figure 2c) is good, but in the layers 3-5 we see horizontal artefacts caused by incorrect Q_P model (Figure 2d). The inversion of Q_P is less accurate. The only upper low-Q_P layer is reconstructed relatively satisfactory. The horizontal artefacts in Q_P reflect significant cross-talk between velocity and attenuation.

Test 2 deals with sequential inversion of spatially correlated v_P and Q_P. The quality of the inverted v_P model in Figure 2e is comparable with the result of Test 1. The reconstructed Q_P model consists of smaller number of horizontal artefacts than in the previous case (Figure 2f).

Test 3 deals with simultaneous inversion of spatially uncorrelated v_P and Q_P. The recovered v_P model in Figure 3c is good, but the number of horizontal artefacts has increased in comparison with Test 1. The Q_P model is poorly reconstructed (Figure 3d). Only the upper low-Q_P layer is resolved relatively satisfactory with the correct position of bottom interface which does not coincide with the interface of the corresponding v_P layer. The lower part of Q_P model consists of numerous horizontal artefacts.

Test 4 deals with sequential inversion of spatially uncorrelated v_P and Q_P. The reconstruction of v_P model (Figure 3e) is very similar to the Test 3. The inverted Q_P model (Figure 3f) is again bad with the only satisfactory reconstruction of the upper low-Q_P layer.

To summarize the 1D experiment, we observe the limited ability of viscoacoustic inversion to reconstruct satisfactory v_P and Q_P models. A reasonable quality factor model is recovered in shallow areas. With increasing depth Q_P is characterized by artefacts, which, however, either do not have a negative impact on the v_P reconstruction or even improve the v_P model.

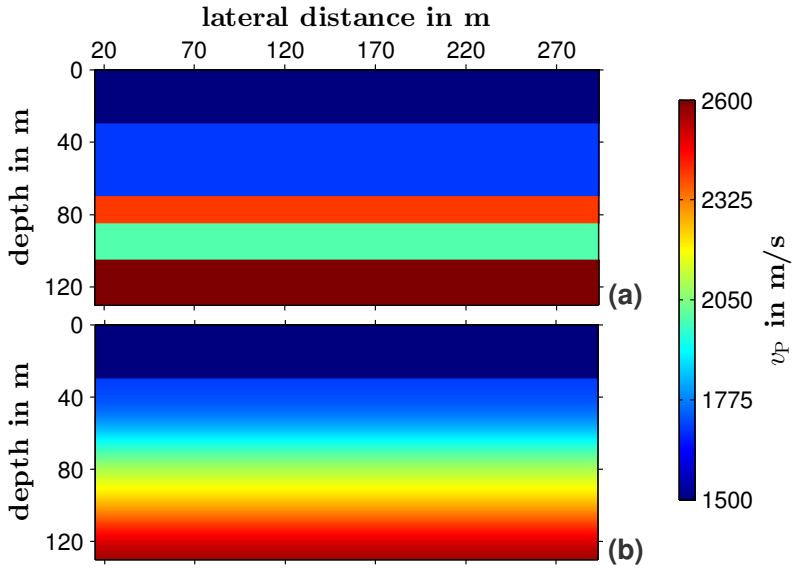

Figure 1: 1D experiment: real (a) and initial (b) v_P model for correlated and uncorrelated inversion tests.

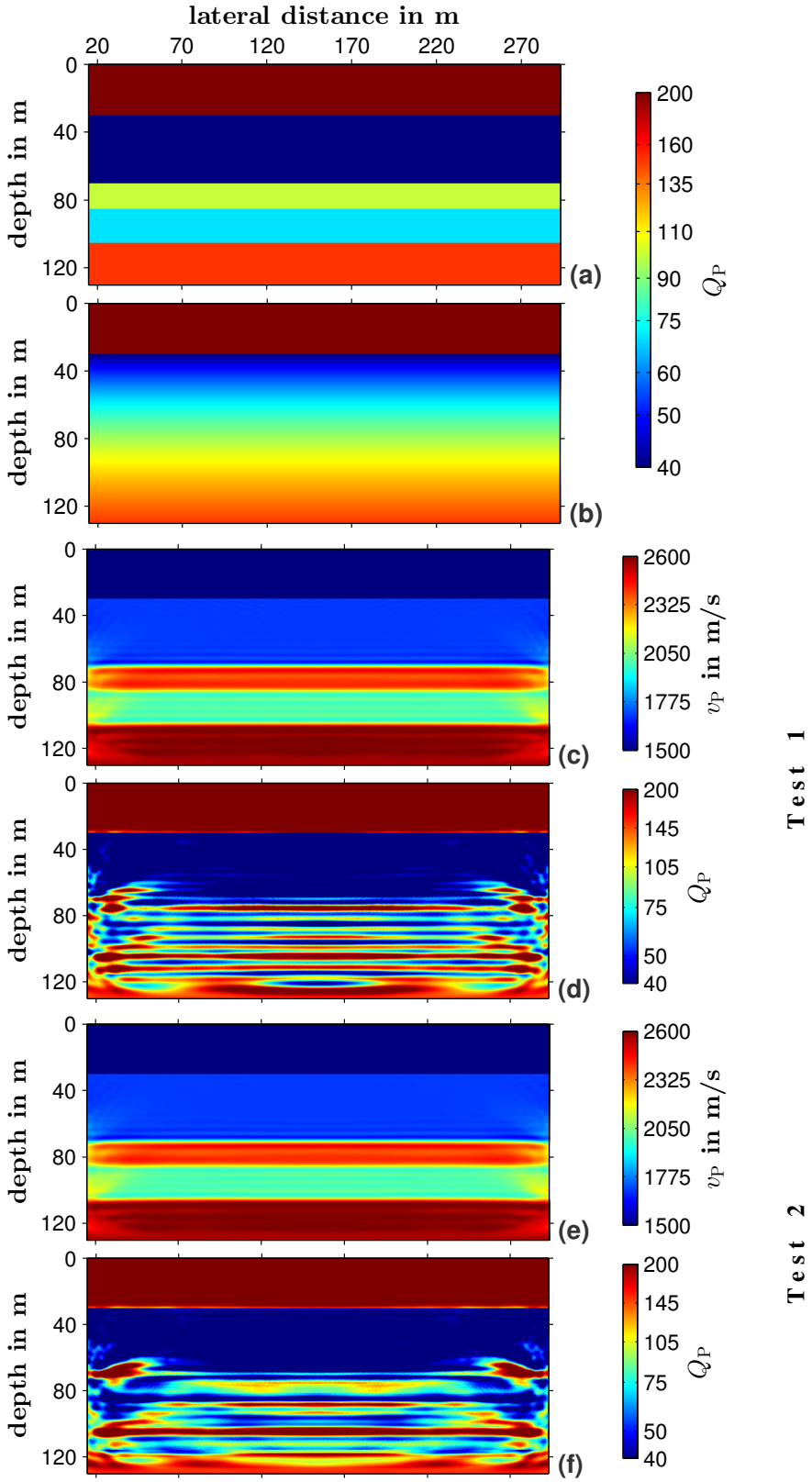

Figure 2: 1D experiment with spatially correlated v_P and Q_P models: Figures show real Q_P model (a), initial Q_P model (b), results of sequential Q_P-v_P inversion (c,d) and results of simultaneous Q_P-v_P inversion (e,f). The first layer is assumed to be known and, thus, not updated.

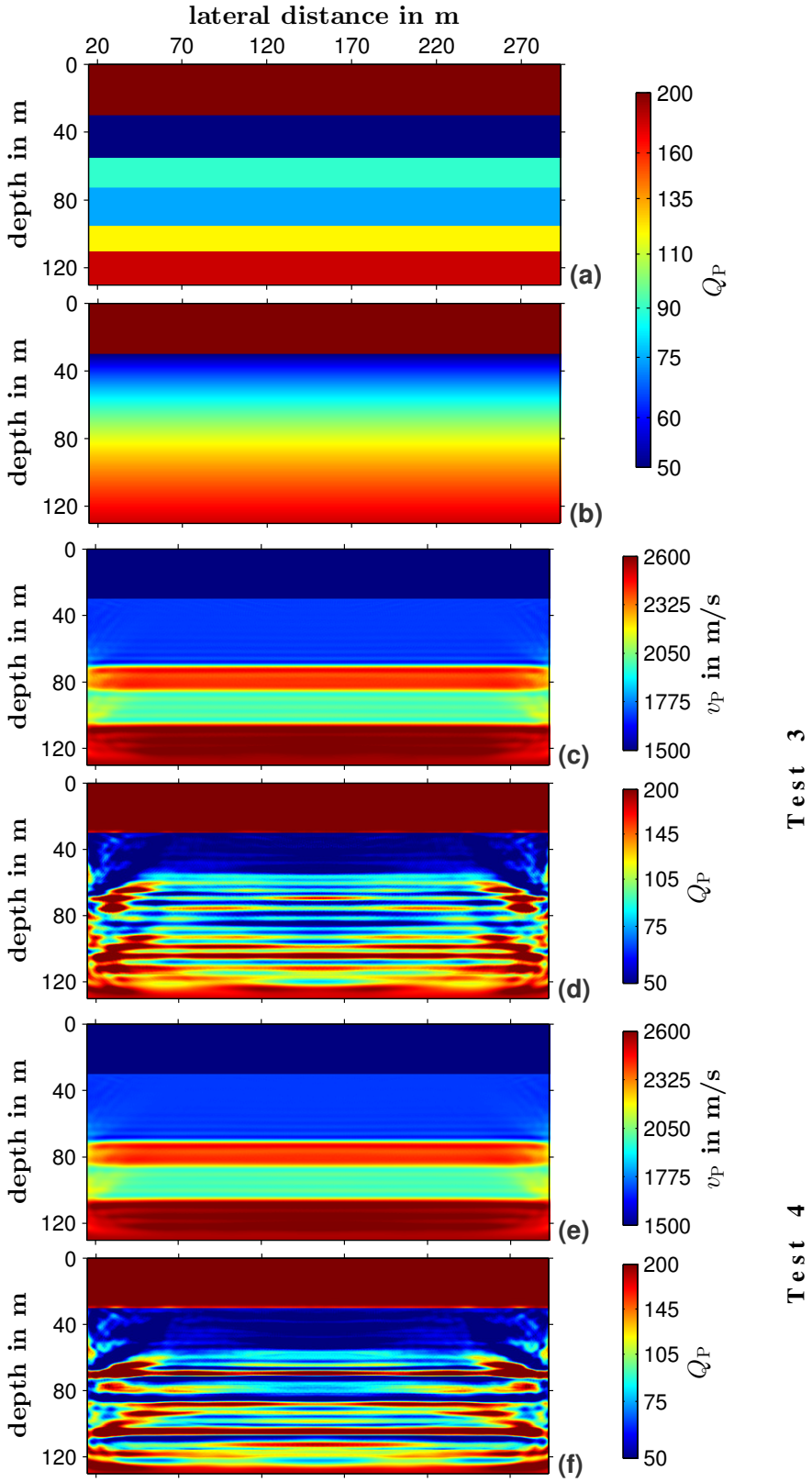

Figure 3: 1D experiment with spatially uncorrelated v_P and Q_P models: Figures show real Q_P model (a), initial Q_P model (b), results of sequential Q_P-v_P inversion (c,d) and results of simultaneous Q_P-v_P inversion (e,f). The first layer is assumed to be known and, thus, not updated.

Synthetic Marmousi experiment

In analogy to the previous section similar investigations are applied to a section of the Marmousi-2 model (Figure 4a) based on Versteeg (1994) and Martin (2002). Hereby the velocities are clipped to the range $v_\mathrm{P} = [1500, 4000]\ \frac{\mathrm{m}}{\mathrm{s}}$ to reduce computational efforts. The acquisition geometry is given by a marine streamer geometry located at the free surface. It consists of 32 explosive sources as well as a maximum number of 300 hydrophones. The source signal consists of a Ricker wavelet with a dominant frequency $f_s = 9$ Hz. The model size is 3000×10000 m which results – using a grid spacing $DH = 5$ m – in a grid size of 600×2000 grid points. Due to the application of a perfectly matched layer (width = 150 m) for avoiding artificial boundary reflections in finite-difference modeling, all model related figures are clipped to the relevant area. Furthermore, the synthetic seismic data is obtained by application of a recording time of 5.145 s with a time discretization of $DT = 7 \cdot 10^{-4}$ s. Again, the approximation of relaxation parameters is based on reference frequency $f_0 = f_s$. In order to consider the relevant frequency content $f = [0,\ 20]$ Hz of the data, we use three relaxation mechanisms with corresponding relaxation frequencies $f_{r,l} = (0.151, 1.93, 18.9)$ Hz.
In analogy to the 1D experiment, we repeat inversion tests investigating the sensitivity of viscoacoustic FWI to inversion strategy (sequential or parallel) and to spatial correlation of v_P and Q_P (cp. Table 2). In order to verify possible improvements achieved by viscoacoustic inversion, we perform a quasi-acoustic reference inversion of viscoacoustic data ("test 0") in case of the correlated problem and using a constant passive Q_P model (cp. Kurzmann, A., 2012). Again, this test configuration requires several input models:

- True (Figure 4a) and initial (Figure 4b) velocity models are used in all tests.
- Tests 0, 1 and 2 with spatial correlation of v_P and Q_P are based on true (Figure 5a) and initial (Figure 5b) Q_P models. The true Q_P-model is derived from the velocity model (Figure 4a) by applying an empirical v_P-Q_P relation (Hamilton, 1972):

$$\frac{1}{Q_\mathrm{P}} = \alpha_\mathrm{P}\ \frac{v_\mathrm{P}}{\pi f - \frac{\alpha_\mathrm{P}^2 v_\mathrm{P}^2}{4\pi f}}. \tag{8}$$

  The intrinsic attenuation α_P is assigned to the structures of the velocity model. We used laboratory α_P values for the frequency range of the given example in marine sedimentary layers (Attewell, 1966). The quality factor ranges from 10 in the shallow sedimentary layers to 280 in deeper high velocity zones. In order to be an appropriate representation of shallow areas, we choose a constant initial $Q_\mathrm{P} = 25$. The corresponding inversion results can be found in Figures 5c (test 0), 5d,e (test 1) and 5f,g (test 2).
- Tests 3 and 4 – with spatially uncorrelated v_P and Q_P models – are based on true (Figure 6a) and initial (Figure 6b) Q_P models. Here, we avoid spatial correlation by turning upside down the subseafloor area of the true Q_P model of Tests 0-2. Consequently, $Q_\mathrm{P} = 100$ is a good initial approximation. The corresponding inversion results can be found in Figures 6c,d (test 3) and 6e,f (test 4).

As shown by Kurzmann, A. (2012), it is important to choose passive Q_P models which are representative for the shallow areas of the sedimentary structures. Therefore, we use different values for initial Q_P models in "correlated" and "uncorrelated" FWI tests.

Table 2: Marmousi experiment: Compilation of all tests.

	spatial correlation of v_P and Q_P	inversion strategy	initial models
Test 0	correlated	v_P only	smooth v_P and constant $Q_\mathrm{P} = 25$
Test 1	correlated	parallel	smooth v_P and constant $Q_\mathrm{P} = 25$
Test 2	correlated	sequential	smooth v_P and constant $Q_\mathrm{P} = 25$
Test 3	uncorrelated	parallel	smooth v_P and constant $Q_\mathrm{P} = 100$
Test 4	uncorrelated	sequential	smooth v_P and constant $Q_\mathrm{P} = 100$

Test 0 deals with single-parameter viscoacoustic v_P inversion with spatially correlated v_P and Q_P models and passive parameter $Q_\mathrm{P} = 25$. The recovered v_P model is very smooth (Figure 5c). This leads to bad fit of the recorded and modelled seismograms as shown in Figure 7a,b. The constant Q_P value is a quite good representation of the upper structures, but shows significant deviations in deeper areas. That results in an increasingly inaccurate v_P reconstruction with increasing depth (cp. Kurzmann et al., 2013).

Test 1 deals with simultaneous inversion of spatially correlated v_P and Q_P. The recovered v_P model (Figure 5d) is much better than in reference Test 0. The inversion of Q_P is only satisfactory in the upper part of the model (Figure 5e). In the lower part of Q_P model there are many artefacts. However, apart from these completely erroneous Q_P values, the location of Q_P structures is quite satisfactory. Here, the footprint of v_P in Q_P is highly probable. Furthermore, the inverted models lead to excellent fit of the recorded and modelled data as shown in Figure 7c,d. Nevertheless, in comparison with Test 0, even an artificial reconstruction of Q_P combined with the spatial correlation to v_P helps to improve the velocity model.

Test 2 deals with sequential inversion of spatially correlated v_P and Q_P. The quality of the inverted v_P (Figure 5f) and Q_P models (Figure 5g) is comparable with the result of Test 1. The reconstructed Q_P model again consists of huge artefacts in the lowest part of the model. Again, we observe an excellent data fit (not shown but comparable with Figure 7c,d).

Test 3 deals with simultaneous inversion of spatially uncorrelated v_P and Q_P. The recovered v_P model is good and comparable to the results with correlated problems (Figure 6c). The Q_P model is poorly reconstructed (Figure 6d). However, we observe the partly reconstruction of high-Q_P layers in shallow areas. In contrast, with increasing depth the strength of the v_P footprint on Q_P increases significantly. The shape of the deepest Q_P structures coincides well with v_P. Test 3 substantiates the observations of Test 1: Due to strong v_P footprints, a reliable interpretation of deeper Q_P areas is not possible. In spite of the artificial Q_P recovery, the data misfit is reduced nearly perfectly (Figure 8) and the velocity model does not show significant negative impacts.

Test 4 deals with sequential inversion of spatially uncorrelated v_P and Q_P. The reconstruction of v_P model in Figure 6e is very similar to the Test 3. The inverted Q_P model is again bad with the only satisfactory reconstruction of the shallow parts (Figure 6f). But again, the inverted models lead to excellent fit of the recorded and modelled data (not shown but comparable to Figure 8). This can be interpreted as low sensitivity of the observed data to deeper parts of attenuation model.

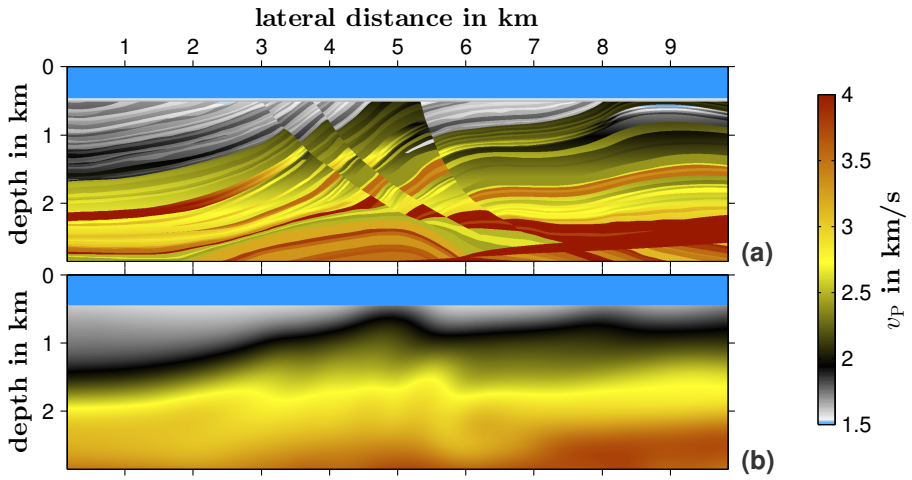

Figure 4: Marmousi experiment: real (a) and initial (b) velocity model for both correlated and uncorrelated Marmousi tests.

To summarize the Marmousi experiment, we observe a fundumental parallelism to the 1D experiment, regarding the depth-dependent quality of the reconstructed Q_P model. Furthermore, the uncorrelated Marmousi problem clearly illustrates the quite satisfactory Q_P reconstruction in shallow areas and the unreliable footprint of v_P in deeper areas due to the cross-talk between both model parameters and a possible insensitivity of seismic data to attenuation.

CONCLUSIONS

In this work we implemented and developed time-domain viscoacoustic full waveform inversion based on rheology of a generalized standard linear solid. We tested its applicability on synthetic reflection marine data using the 1D layered and 2D Marmousi models. In contrast to the most of existing studies, we considered both spatially correlated and spatially uncorrelated models of velocity and attenuation. In all examples v_P is well recovered, but Q_P is satisfactorily inverted only in the upper part of models. Although the lowest parts of attenuation models are poorly resolved, the comparison of the recorded and modelled seismograms show excellent fit in all cases. This can be interpreted either as low sensitivity of the given synthetic data to lower parts of attenuation model or a cross-talk effect where the attenuation-related data misfit is explained by the velocity model. However, the Marmousi experiment illustrates the improvement of the velocity reconstruction by the satisfactory Q_P recovery in shallow areas and even by artificial quality factors in deeper parts. From the interlaced multi-stage FWI workflow consisting of multi-scale inversion and v_P-Q_P inversion strategies, we obtained results with comparable accuracy for both parallel and sequential inversion strategies.

In viscoacoustic inversion, the conventional assumption of correlated velocity and attenuation subsurface structures might induce an incorrect interpretation. Indeed, using the conventional assumption, the inverted low Q_P anomalies in the lowest part of model (Marmousi Test 3 and Test 4) would be interpreted as true anomalies rather artefacts.

On the one hand, the preliminary Q_P results in this work make clear that further development of inversion strategies is necessary to extract the desired attenuation information from seismic data. On the other hand, the investigation of multiparameter inverse problems with (highly) spatially-uncorrelated parameters has to be considered as a necessary step to verify the reliability of results obtained by those inversion strategies.

ACKNOWLEDGMENTS

This work was kindly supported by the sponsors of the Wave Inversion Technology (WIT) Consortium. Furthermore, we are grateful for using the supercomputers JUROPA at Jülich Supercomputing Centre and ForHLR at Steinbuch Centre for Computing (KIT, Karlsruhe; funded by the state of Baden-Württemberg and the federal state of Germany). Renat Shigapov was kindly supported by German-Russian Interdisciplinary Science Center (G-RISC).

REFERENCES

Alford, R. M., Kelly, K. R., and Boore, D. M. (1974). Accuracy of finite-difference modeling of the acoustic wave equation. *Geophysics*, 39(6):834–842.

Askan, A., Akcelik, V., Bielak, J., and Ghattas, O. (2007). Full waveform inversion for seismic velocity and anelastic losses in heterogeneous structures. *Bulletin of the Seismological Society of America*, 97(6):1990–2008.

Askan, A., Akcelik, V., Bielak, J., and Ghattas, O. (2010). Parameter sensitivity analysis of a nonlinear least-squares optimization-based anelastic full waveform inversion method. *Comptes Rendus Mécanique*, 338(7-8):364–376. Inverse problems.

Askan, A. and Bielak, J. (2008). Full anelastic waveform tomography including model uncertainty. *Bulletin of the Seismological Society of America*, 98(6):2975–2989.

Assimaki, D., Kallivokas, L., Kang, J., Li, W., and Kucukcoban, S. (2012). Time-domain forward and inverse modeling of lossy soils with frequency-independent q for near-surface applications. *Soil Dynamics and Earthquake Engineering*, 43(0):139–159.

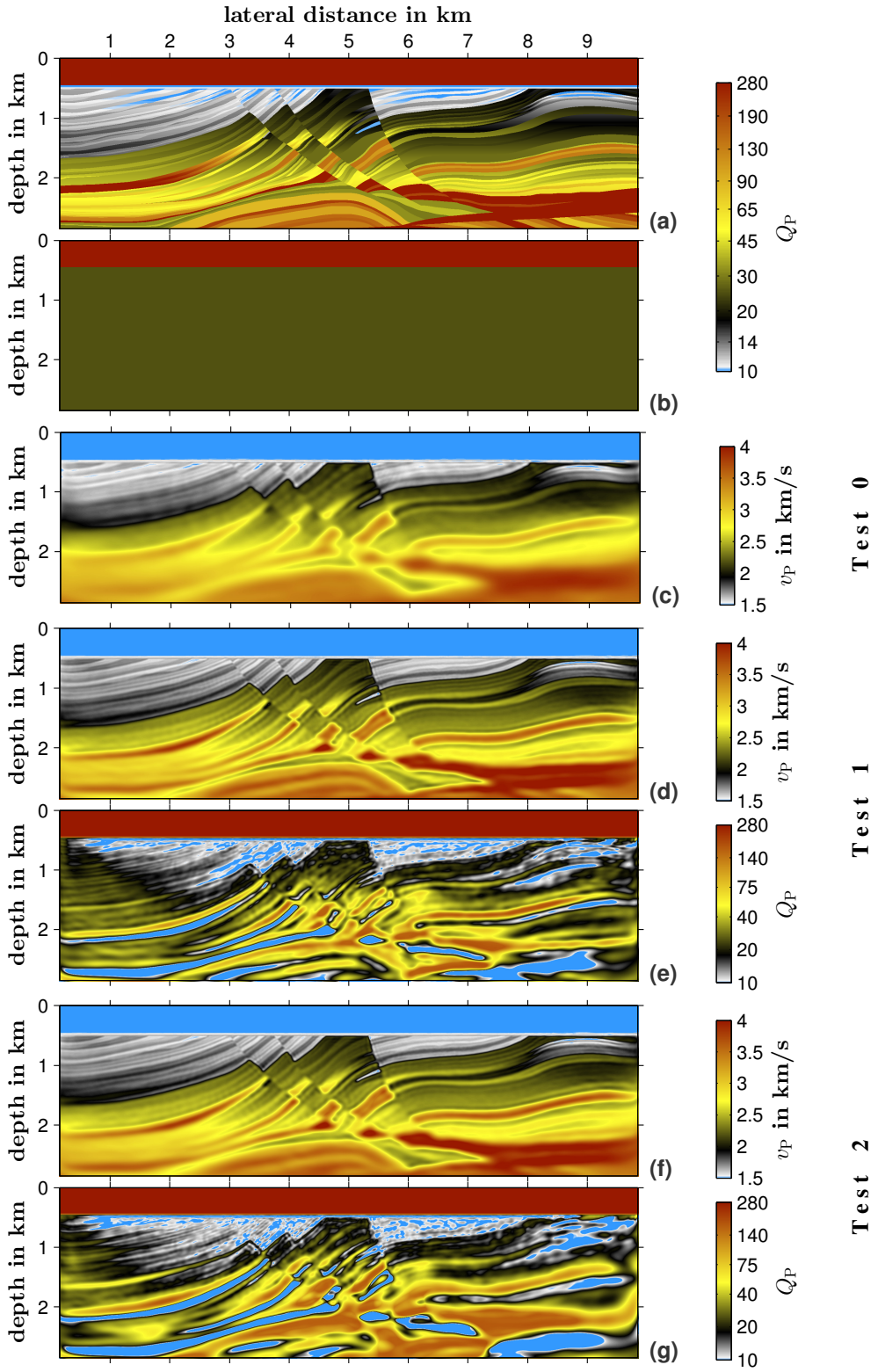

Figure 5: Marmousi experiment with spatially correlated v_P and Q_P models: Figures show real Q_P model (a), initial (Test 1 and Test 2) / passive (test 0) Q_P model (b), result of reference inversion using constant passive Q_P (c), results of sequential Q_P-v_P inversion (d,e) and results of simultaneous Q_P-v_P inversion (f,g). In the water column we define acoustic conditions: $Q_P = 60000$.

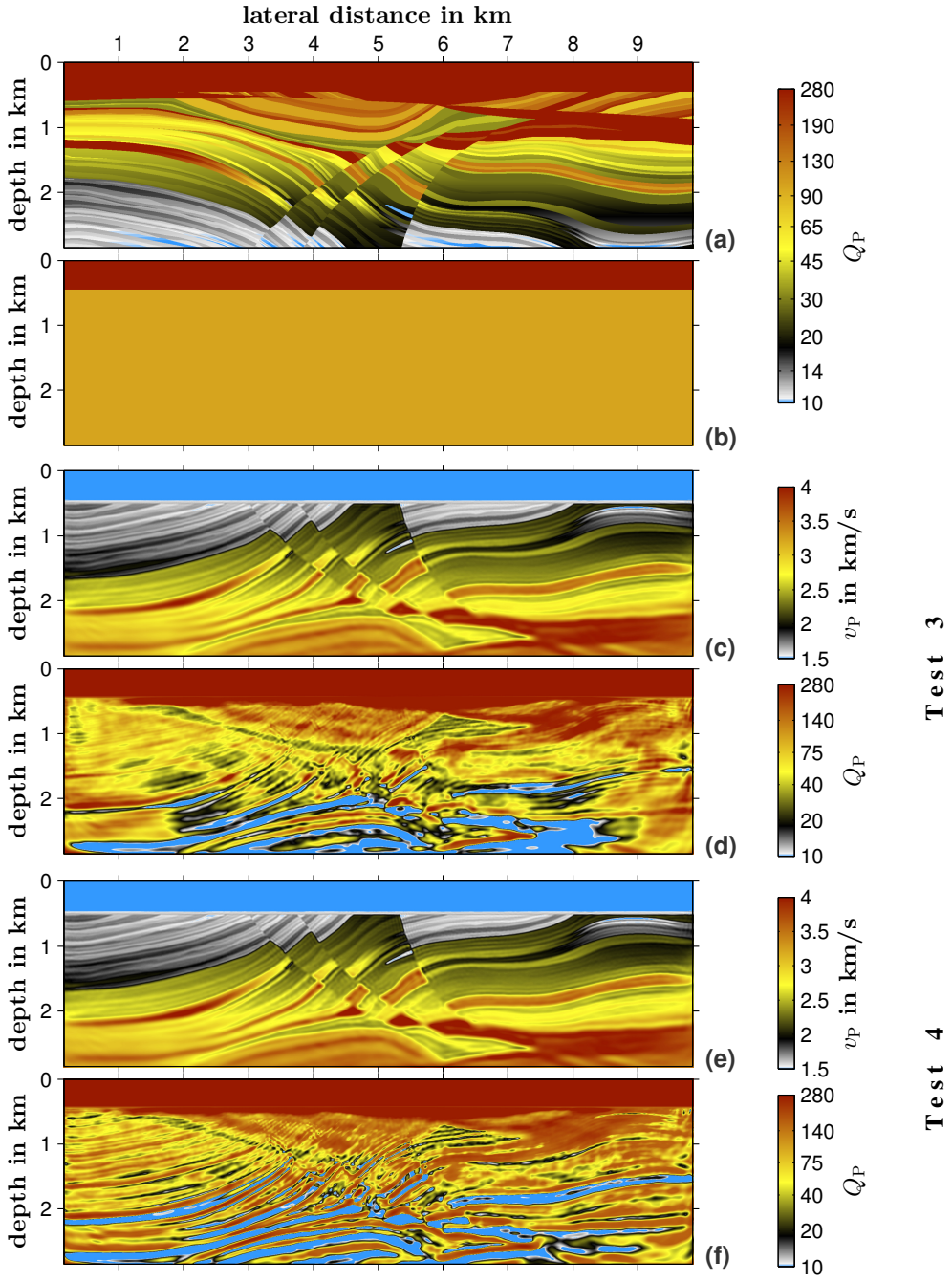

Figure 6: Marmousi experiment with spatially uncorrelated v_P and Q_P models: Figures show real Q_P model (a), initial Q_P model (b), results of sequential Q_P-v_P inversion (c,d) and results of simultaneous Q_P-v_P inversion (e,f). In the water column we define acoustic conditions: $Q_P = 60000$.

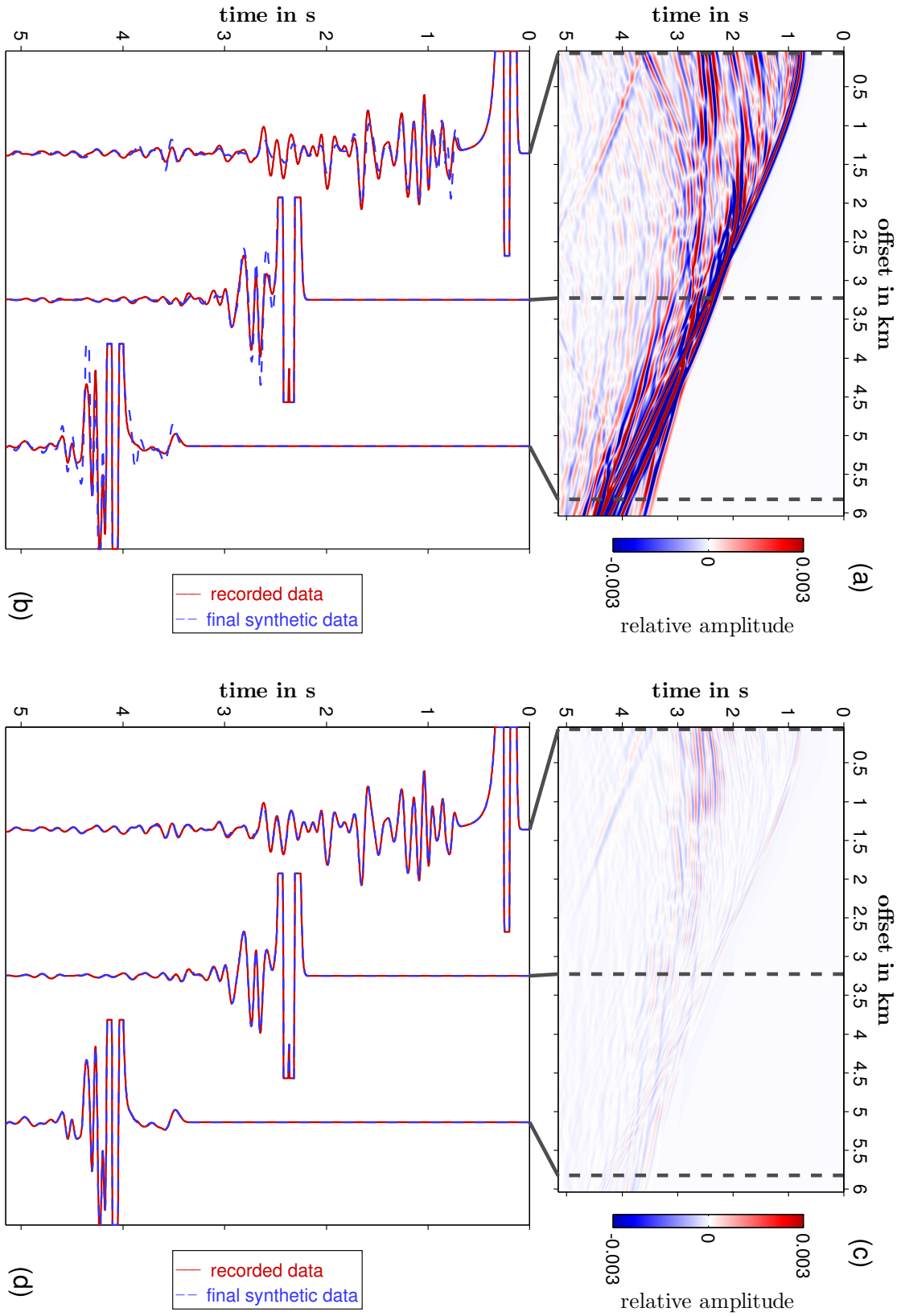

Figure 7: Test 0 (a,b) and Test 1 (c,d) of Marmousi experiment with spatially correlated v_{P} and Q_{P} models: Figures b) and d) show both recorded and synthetic data of the inversion result at exemplary offsets for a representative shot located at $x = 2.555$ km. As an indication of the data misfit, Figures a) and c) illustrate the residuals between recorded and final synthetic data.

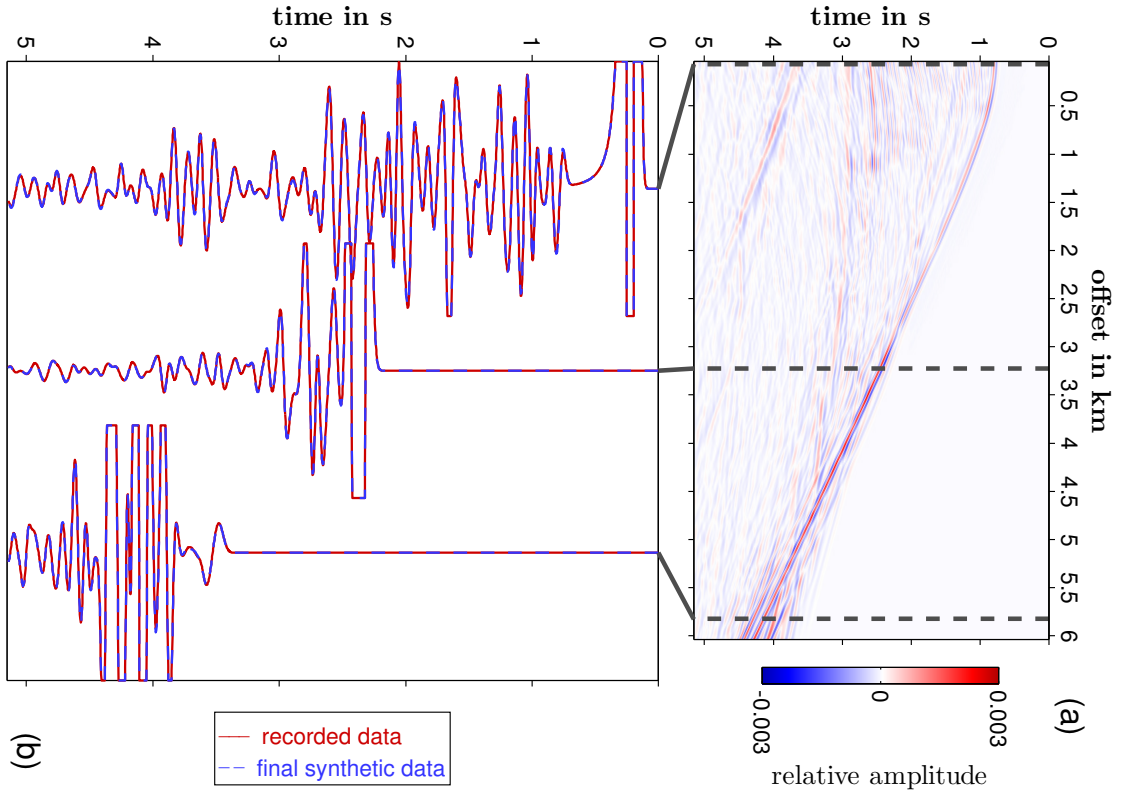

Figure 8: Test 3 of Marmousi experiment with spatially uncorrelated v_{P} and Q_{P} models: Figure b) and d) show both recorded and synthetic data of the inversion result at exemplary offsets for a representative shot located at $x = 2.555$ km. As an indication of the data misfit, Figures a) and c) illustrate the residuals between recorded and final synthetic data.

Attewell, P. B. & Ramana, Y. V. (1966). Wave attenuation and internal friction as functions of frequency in rocks. *Geophysics*, 31:1049–1056.

Bai, J., Yingst, D., Bloor, R., and Leveille, J. (2014). Viscoacoustic waveform inversion of velocity structures in the time domain. *Geophysics*, 79(3):R103–R119.

Berenger, J. P. (1994). A Perfectly Matched Layer for the Absorption of Electromagnetic Waves. *Journal of Computational Physics*, 114:185–200.

Blanch, J., Robertsson, J., and Symes, W. (1995). Modeling of a constant q: Methodology and algorithm for an efficient and optimally inexpensive viscoelastic technique. *Geophysics*, 60(1):176–184.

Bohlen, T. (2002). Parallel 3D viscoelastic finite difference seismic modelling. *Computers and Geosciences*, 28:887–899.

Brossier, R. (2011). Two-dimensional frequency-domain visco-elastic full waveform inversion: Parallel algorithms, optimization and performance. *Comput. Geosci.*, 37(4):444–455.

Bunks, C., Saleck, F. M., Zaleski, S., and Chavent, G. (1995). Multiscale seismic waveform inversion. *Geophysics*, 60(5):1457–1473.

Carcione, J. (2007). *Wave Fields in Real Media: Wave Propagation in Anisotropic, Anelastic, Porous and Electromagnetic Media*. Handbook of Geophysical Exploration: Seismic Exploration. Elsevier Science.

Carcione, J. M., Kosloff, D., and Kosloff, R. (1988). Wave propagation simulation in a linear viscoacoustic medium. *Geophysical Journal International*, 93(2):393–401.

Causse, E., Mittet, R., and Ursin, B. (1999). Preconditioning of fullâĂŘwaveform inversion in viscoacoustic media. *Geophysics*, 64(1):130–145.

Charara, M., Barnes, C., and Tarantola, A. (2000). Full waveform inversion of seismic data for a viscoelastic medium. In Hansen, P., Jacobsen, B., and Mosegaard, K., editors, *Methods and Applications of Inversion*, volume 92 of *Lecture Notes in Earth Sciences*, pages 68–81. Springer Berlin Heidelberg.

Chew, W. C. and Weedon, W. H. (1994). A 3D perfectly matched medium from modified Maxwell's equations with stretched coordinates. *Microwave and Optical Technical Letters*, 7(13):599–604.

Emmerich, H. and Korn, M. (1987). Incorporation of attenuation into time-domain computations of seismic wave fields. *Geophysics*, 52(9):1252–1264.

Fichtner, A., Kennett, B. L. N., Igel, H., and Bunge, H. (2009). Full seismic waveform tomography for upper-mantle structure in the Australasian region using adjoint methods. *Geophysical Journal International*, 179:1703–1725.

Hak, B. and Mulder, W. A. (2011). Seismic attenuation imaging with causality. *Geophysical Journal International*, 184(1):439–451.

Hamilton, E. L. (1972). Compressional-wave attenuation in marine sediments. *Geophysics*, 37(4):620–646.

Hicks, G. and Pratt, R. (2001). Reflection waveform inversion using local descent methods: Estimating attenuation and velocity over a gas-sand deposit. *Geophysics*, 66(2):598–612.

Igel, H., Djikpéssé, H., and Tarantola, A. (1996). Waveform inversion of marine reflection seismograms for P impedance and Poisson's ratio. *Geophysical Journal International*, 124:363–371.

Kamei, R. and Pratt, R. G. (2013). Inversion strategies for visco-acoustic waveform inversion. *Geophysical Journal International*, 194(2):859–884.

Knopoff, L. (1964). Q. *Reviews of Geophysics*, 2(4):625–660.

Kurzmann, A., Köhn, D., Przebindowska, A., Nguyen, N., and Bohlen, T. (2009). 2D Acoustic Full Waveform Tomography: Performance and Optimization. In *Extended Abstracts, 71st Conference and Technical Exhibition*. EAGE.

Kurzmann, A., Przebindowska, A., Köhn, D., and Bohlen, T. (2013). Acoustic full waveform tomography in the presence of attenuation: a sensitivity analysis. *Geophysical Journal International*, 195(2):985–1000.

Kurzmann, A., Przebindowska, A., B. (2012). On the importance of attenuation in acoustic waveform tomography of marine seismic data. In *Annual Report No. 15 of the Wave Inversion Technology Consortium*.

Lailly, P. (1983). The seismic inverse problem as a sequence of before stack migrations. In *Conference on inverse scattering: theory and application*, pages 206–220. Society for Industrial and Applied Mathematics, Philadelphia, PA.

Liao, Q. and McMechan, G. (1996). Multifrequency viscoacoustic modeling and inversion. *Geophysics*, 61(5):1371–1378.

Liu, C., Gao, F., Feng, X., Liu, Y., and Liu, Y. (2013). Incorporating attenuation effects into frequency-domain full waveform inversion from zero-offset vsp data from the stokes equation. *Journal of Geophysics and Engineering*, 10(3):035004.

Liu, H.-P., Anderson, D. L., and Kanamori, H. (1976). Velocity dispersion due to anelasticity; implications for seismology and mantle composition. *Geophysical Journal International*, 47(1):41–58.

Long, G., Li, X., Zhang, M., and Zhu, T. (2009). Visco-acoustic transmission waveform inversion of velocity structure in space-frequency domain. *Earthquake Science*, 22(1):45–52.

Malinowski, M., Operto, S., and Ribodetti, A. (2011). High-resolution seismic attenuation imaging from wide-aperture onshore data by visco-acoustic frequency-domain full-waveform inversion. *Geophysical Journal International*, 186(3):1179–1204.

Martin, G. (2002). Marmousi-2: An updated model for the investigation of AVO in structurally complex areas. In *Expanded abstracts, 72nd Annual International Meeting*. SEG.

Mora, P. (1987). Nonlinear two-dimensional elastic inversion of multioffset data. *Geophysics*, 52(9):1211–1228.

Müller, T., Gurevich, B., and Lebedev, M. (2010). Seismic wave attenuation and dispersion resulting from wave-induced flow in porous rocks – a review. *Geophysics*, 75(5):75A147–75A164.

Plessix, R.-E. (2006). A review of the adjoint-state method for computing the gradient of a functional with geophysical applications. *Geophysical Journal International*, 167(2):495–503.

Prieux, V., Brossier, R., Operto, S., and Virieux, J. (2013). Multiparameter full waveform inversion of multicomponent ocean-bottom-cable data from the valhall field. part 1: imaging compressional wave speed, density and attenuation. *Geophysical Journal International*, 194(3):1640–1664.

Ren, Z., Liu, Y., and Zhang, Q. (2014). Multiscale viscoacoustic waveform inversion with the second generation wavelet transform and adaptive time-space domain finite-difference method. *Geophysical Journal International*.

Robertsson, J., Blanch, J., and Symes, W. (1994). Viscoelastic finite-difference modeling. *Geophysics*, 59(9):1444–1456.

Shapiro, S. and Hubral, P. (1999). *Elastic waves in random media: fundamentals of seismic stratigraphic filtering*. Lecture notes in earth sciences. Springer.

Sirgue, L. and Pratt, R. G. (2004). Efficient waveform inversion and imaging: A strategy for selecting temporal frequencies. *Geophysics*, 69(1):231–248.

Song, Z., Williamson, P., and Pratt, R. (1995). Frequency-domain acoustic-wave modeling and inversion of crosshole data: Part ii – inversion method, synthetic experiments and real-data results. *Geophysics*, 60(3):796–809.

Takougang, E. M. T. and Calvert, A. J. (2013). Seismic waveform tomography across the seattle fault zone in puget sound: resolution analysis and effectiveness of visco-acoustic inversion of viscoelastic data. *Geophysical Journal International*, 193(2):763–787.

Tarantola, A. (1984). Inversion of seismic reflection data in the acoustic approximation. *Geophysics*, 49(8):1259–1266.

Tarantola, A. (1988). Theoretical background for the inversion of seismic waveforms including elasticity and attenuation. *pure and applied geophysics*, 128(1-2):365–399.

Versteeg, R. (1994). The Marmousi experience: Velocity model determination on a synthetic complex data set. *The Leading Edge*, 13:927–936.

Virieux, J. and Operto, S. (2009). An overview of full-waveform inversion in exploration geophysics. *Geophysics*, 74(6):WCC1–WCC26.

Watanabe, T., Nihei, K. T., Nakagawa, S., and Myer, L. R. (2004). Viscoacoustic wave form inversion of transmission data for velocity and attenuation. *The Journal of the Acoustical Society of America*, 115(6):3059–3067.